Electronic Supplementary Material (ESI) for Journal of Materials Chemistry C.

Reducing the cyan-cavity: $Lu_2MAl_4SiO_{12}:Ce^{3+}$ (M = Mg, Ca, Sr and Ba) phosphor-in-glass film towards full-spectrum laser-driven lighting

Pengfei Wang,[ad] Hang Lin,[*abc] Shisheng Lin,[a] Ping Sui,[ad] Ju Xu,[a] Yao Cheng,[a] Yuansheng Wang[*a]

[a] Key Laboratory of Optoelectronic Materials Chemistry and Physics, Fujian Institute of Research on the Structure of Matter, Chinese Academy of Sciences, Fuzhou, Fujian, 350002, China.

[b] Engineering Research Center of Advanced Glass Manufacturing Technology, Ministry of Education, Donghua University, Shanghai 201620, China.

[c] Fujian Science & Technology Innovation Laboratory for Optoelectronic Information of China, Fuzhou, Fujian, 350108, China.

[d] College of Chemistry and Materials Science, Fujian Normal University, Fujian, Fuzhou, 350007, China.

E-mail: lingh@fjirsm.ac.cn; Tel/Fax: +86-591-63179423
E-mail: yswang@fjirsm.ac.cn; Tel/Fax: +86-591-63179438

Supplementary Note S1:

According to the model proposed by Morrison and developed by Dorenbos, the centroid shift (ε_c) of Ce^{3+} 5d levels is positively correlated with the anion polarizability (α_{sp}). The anion polarizability in Ce^{3+}-doped oxide compounds can be estimated by

$$\alpha_{sp} = 0.33 + \frac{4.8}{\chi^2} \quad (1)$$

Therefore, the anion polarizability is influenced by the average electronegativity χ_{av} of the cations, defined as follows:

$$\chi_{av} = \frac{1}{N_a}\sum_{1}^{N_c}\frac{z_i\chi_i}{\gamma_i} \quad (2)$$

where N_c is the sum of all cations in the compound; N_a is the number of anions in the formula; χ_i represents the electronegativity of cation i with formal charge z_i, and γ is the formal negative charge of the anion. The χ_{av} values of M= Mg, Ca, Sr and Ba in LMAS:Ce^{3+} were calculated to be 1.548, 1.523, 1.518 and 1.513, respectively, by using the Pauling-type electronegativity values and Equation S2. According to Equation S1, a decrease in χ_{av} will lead to an increase in the anion polarizability α_{sp}. As a result, the ε_c follows LMgAS<LCaAS<LSrAS<LBaAS.

Supplementary Note S2:

Dorenbos suggested that the crystal field splitting in the 5d orbital of Ce^{3+} is independent of the centroid shift. Furthermore, the magnitude of the crystal field splitting was said to depend strongly on the coordination geometry rather than on the type of anion present. An empirical correlation between the shape of the first anion coordination polyhedron and the crystal field splitting can be deduced as

$$\varepsilon_{cfs} = \beta_{poly}^{Q} R_{av}^{-2} \quad (3)$$

$$R_{av} = \frac{1}{N}\sum_{1}^{N}(R_i - 0.6\Delta R) \quad (4)$$

where β_{poly}^{Q} is a constant determined by the type of the coordination polyhedron and the charge valence of the lanthanide. R_i is the bond length between the luminescence center and its N coordinated anions in the unrelaxed lattice. ΔR indicates the radius difference between the lanthanide dopant and the host cation. Note that $0.6\Delta R$ represents a pseudorelaxation in bond length.

When the M^{2+} replaces Lu^{3+}, the MO_8 polyhedron will expand as the radius of M^{2+} increases, and at the same time this leads to a decrease in the Ce-O bond length in CeO_8. Since the R_i in LMAS:Ce^{3+} follows Mg>Ca>Sr>Ba, the R_{av} should follow Mg>Ca>Sr>Ba according to Equation S4. Therefore, the ε_{cfs} in LMAS:Ce^{3+} follows Mg<Ca<Sr<Ba(Equation S3).

Supplementary Note S3:

According to the study of Wu et al. (Chem. Phys. Lett. 2007, 441, 250), the lattice distortion extent in Ce^{3+}-doped garnets can be evaluated by a ratio of the O-O bond distances d_{88} and d_{81}(d_{88}/d_{81}). d_{88} represents an O-O bond distance that is shared with an adjacent dodecahedron, while d_{81} represents an O-O bond distance shared with an adjacent tetrahedron. Table s2 below lists the values of d_{88} and d_{81} derived from the XRD Rietveld refinements on LMAS:Ce^{3+} phosphors. There is no obvious change in d_{88}/d_{81}, indicating no obvious lattice distortion occurred in LMAS:Ce^{3+} when M changes from Mg to Ba. Therefore, the reduced Stokes shift should be the major influencing factor for the blue shift.

Supplementary Note S4:

CASN:Eu^{2+} is introduced into PiG as the red supplement. As suggested, we performed some experiments to show if the CASN:Eu^{2+} red-emitting phosphor is thermally degraded after sintering. XRD analyses on CASN:Eu PiG demonstrate the retain of CASN:Eu in glass matrix after co-sintering and no new impurity phases produced (Fig. S9). However, both of the luminescent decay lifetime and quantum efficiency get decreased, which indicate thermal degradation of CASN:Eu (Fig. S10). Attempting to reveal the latent degradation mechanism, an additional experiment was performed by directly heating CASN:Eu phosphor powders to temperature identical to the co-sintering temperature (690 °C) and holding for the same duration (30 min). The measured luminescence decay curve and QE before/after heating are presented in Fig. S11. Upon heating, the calculated lifetime decreases from 660 ns to 604 ns, and the QE decreases from 87% to 55%. Correlating with the results of CASN:Eu PiG (lifetime: 577 ns and QE: 33%), one can deduce that both the thermal degradation in CASN:Eu itself (due to high vaporization ability of N) and the thermal corrosion via interfacial reaction between CASN:Eu and glass play an equivalent role in the luminescent loss. In future work, we will attempt to minimize the thermal degradation effect in CASN:Eu^{2+} by more rational glass composition design or adopting a rapid-sintering technique. To be mentioned, the relatively poor CASN:Eu^{2+} luminescent performance does not influence the core results of this work.

Table S1. Refined results of LMAS:Ce^{3+} phosphor powders.

phosphor type	LMgAS:Ce^{3+}	LCaAS:Ce^{3+}	LSrAS:Ce^{3+}	LBaAS:Ce^{3+}
Space group		$Ia\bar{3}d$		
α=β=γ(°)		90		
a=b=c(Å)	11.8865	11.9188	11.9193	11.9195
V(Å^3)	1679.411	1693.178	1693.396	1693.462
R_{wp}	5.52	5.68	6.52	7.77
R_p	3.91	4.06	7.64	5.79
χ^2	3.28	3.22	5.78	4.58

Table S2. The calculated d_{88}/d_{81} of the LMAS:Ce^{3+} phosphors derived from the XRD Rietveld refinement.

phosphor type	d_{88}(Å)	d_{81}(Å)	d_{88}/d_{81}
LMgAS	2.7457	2.8724	0.95589
LCaAS	2.7532	2.8802	0.95591
LSrAS	2.6347	2.7533	0.95692
LBaAS	2.7534	2.8803	0.95594

Table S3. Full Set of 15 CRIs and the General Ra of LBaAS:Ce^{3+}+CASN:Eu^{2+} PiGF-on-SP (C:R = 15:1) under 1 W/mm^2 blue laser excitation.

R_a	R_1	R_2	R_3	R_4	R_5	R_6	R_7
90.1	90	92	87	90	93	82	90
R_8	R_9	R_{10}	R_{11}	R_{12}	R_{13}	R_{14}	R_{15}

92	80	85	87	60	90	92	93

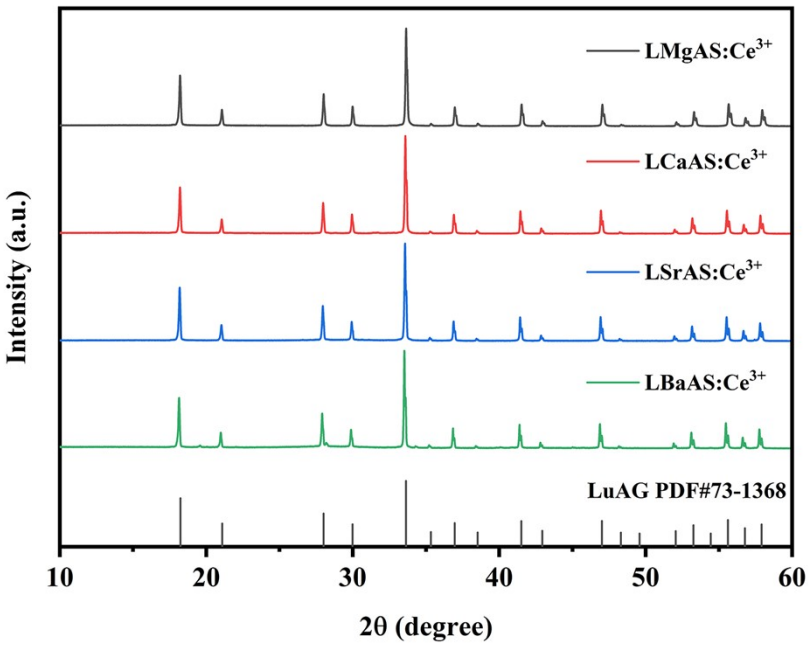

Fig. S1. XRD patterns of the LMAS:Ce^{3+} phosphor powders.

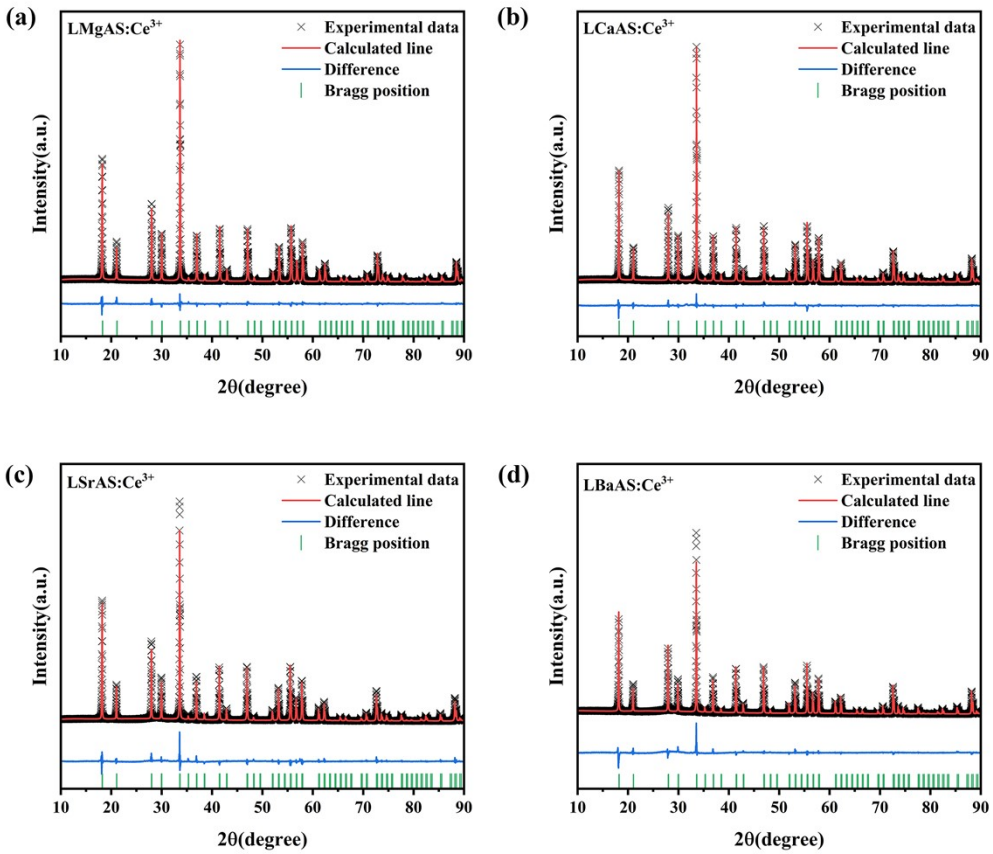

Fig. S2. Rietveld refinement of XRD patterns for LMAS:Ce^{3+} phosphor powders.

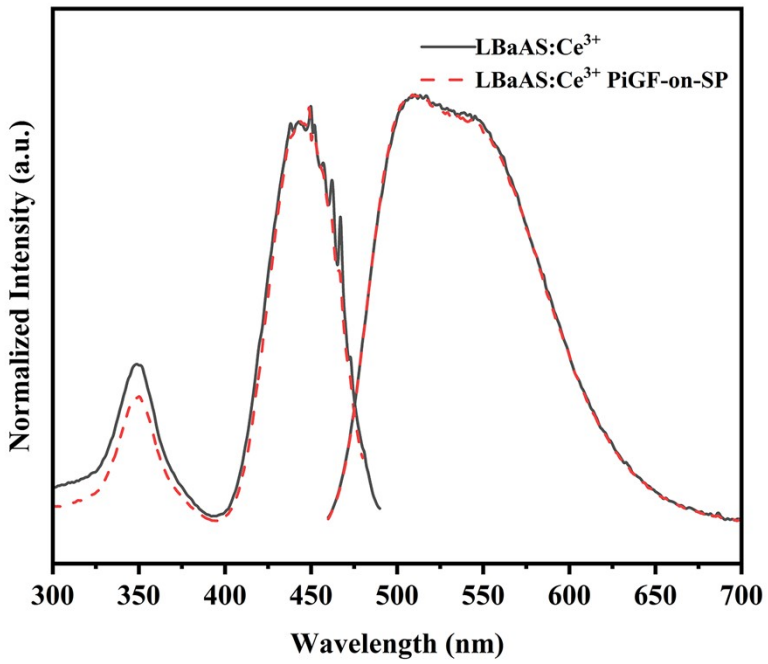

Fig. S3. PLE and PL spectra of LBaAS:Ce^{3+} phosphor powder and the corresponding PiGF-on-SP sample.

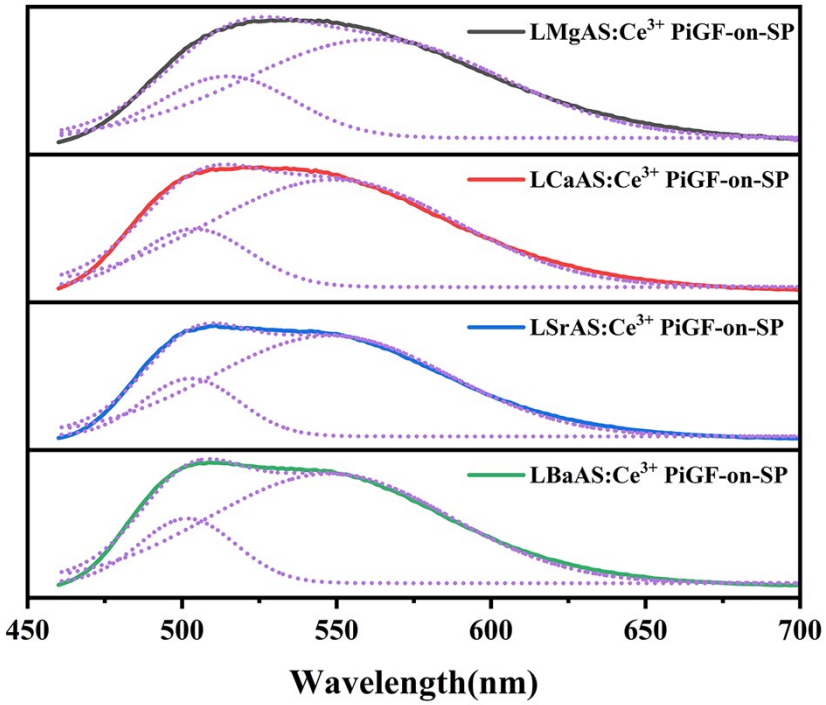

Fig. S4. The Gaussian fitting for the PL spectra of LMAS:Ce^{3+} PiGF-on-SP.

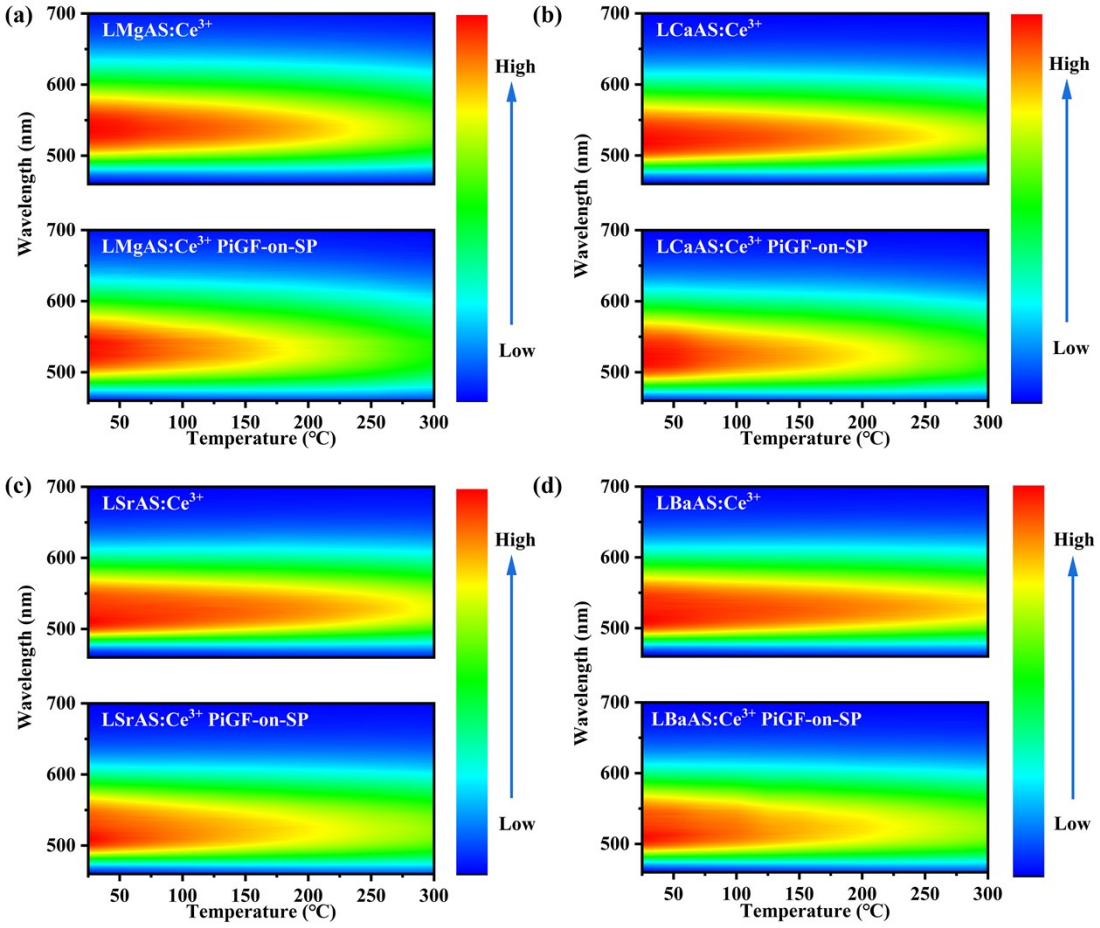

Fig. S5. 2D-contour plot of temperature-dependent PL spectra for (a) LMgAS:Ce^{3+} and LMgAS:Ce^{3+} PiGF-on-SP, (b) LCaAS:Ce^{3+} and LCaAS:Ce^{3+} PiGF-on-SP, (c) LSrAS:Ce^{3+} and LSrAS:Ce^{3+} PiGF-on-SP and (d) LBaAS:Ce^{3+} and LBaAS:Ce^{3+} PiGF-on-SP.

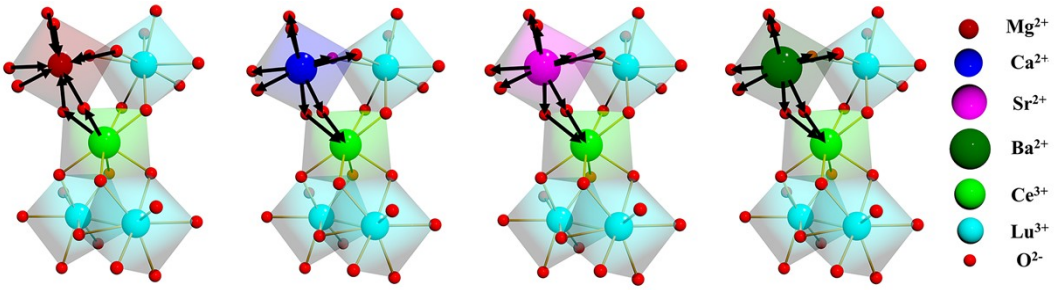

Fig. S6. Schematic diagram of the effect of the change in M cation size on the Ce-O bond

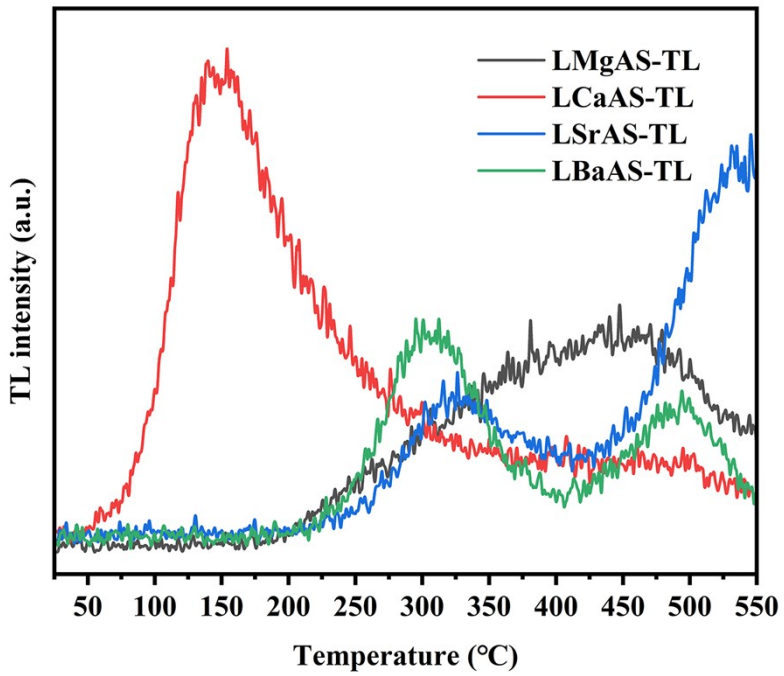

Fig. S7. TL glow curves of LMAS:Ce^{3+} (M=Mg, Ca, Sr and Ba) measured after 450 nm excitation at 300 K for 5 min. The monitored emission wavelengths are 537, 522, 511 and 509 nm, respectively.

Thermoluminescence (TL) spectrum is an effective tool to probe trap properties. TL peak position and TL integrated intensity are correlated with the trap depth and trap concentration, respectively. In Figure S7, TL spectra of LMAS:Ce^{3+} (M=Mg, Ca, Sr and Ba) were measured and compared with each other. There is no obvious regularity, therefore it is hard to ascertain the contribution from defects. However, LBaAS shows the lowest trap concentrations which may be responsible for its highest IQE.

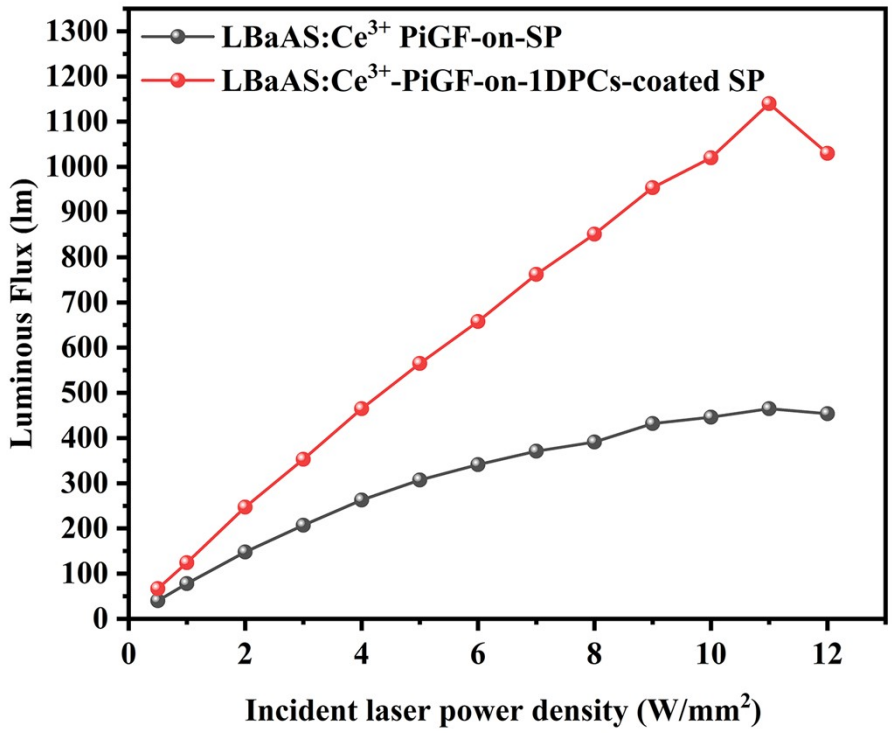

Fig. S8. P_{in} dependent luminous flux of samples in the presence/abscence of 1DPCs film.

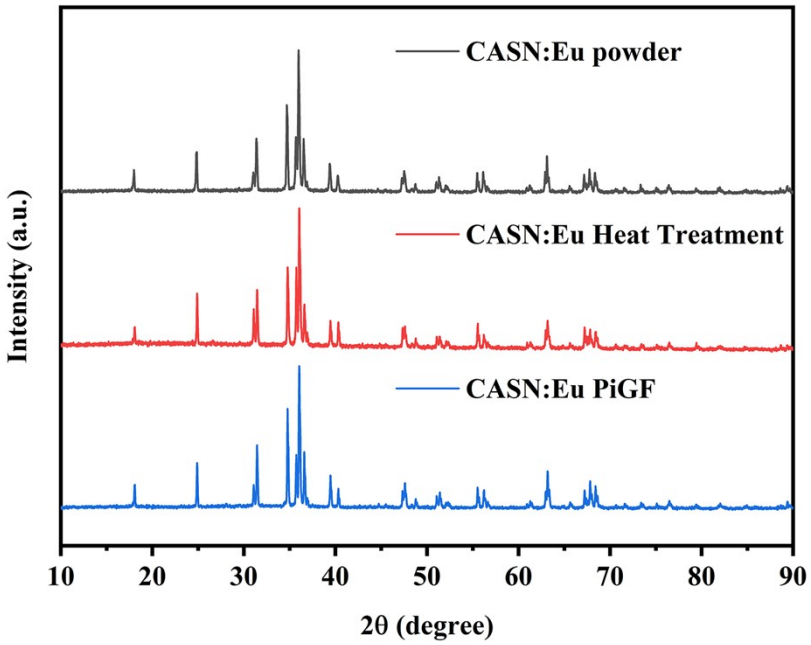

Fig. S9. XRD patterns of CASN:Eu phosphor powders before/after heat treatment at 690 °C for 30 min and CASN:Eu PiGF.

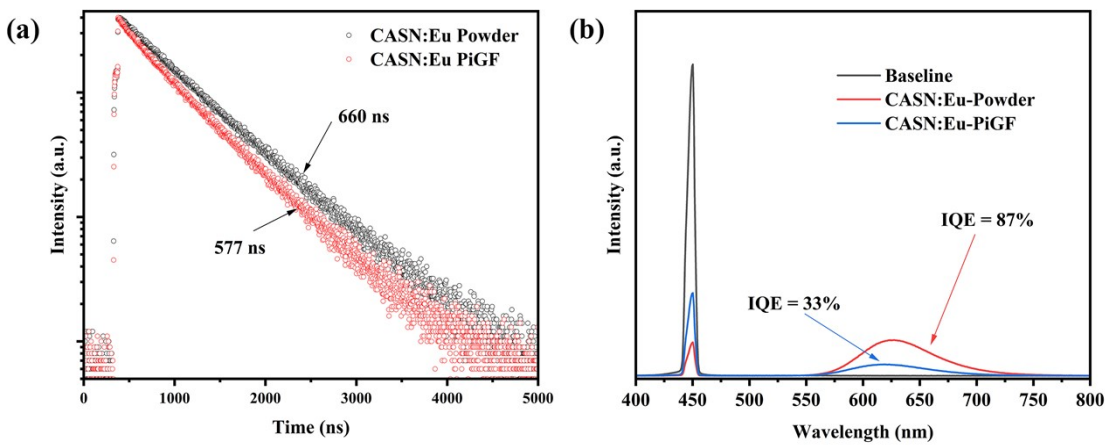

Fig. S10. Comparisons made on luminescent decay curves and QEs of CASN:Eu phosphor powders and CASN:Eu PiGF.

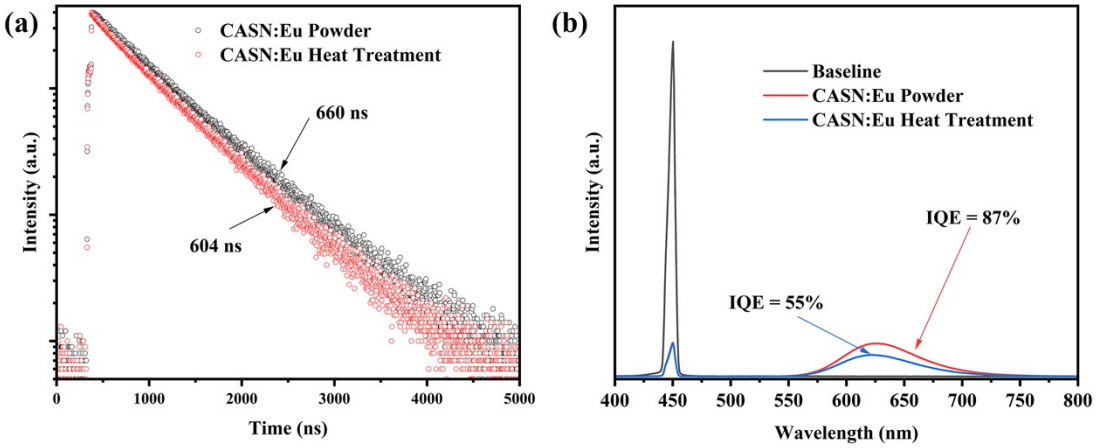

Fig. S11. Comparisons made on luminescent decay curves and QEs of CASN:Eu phosphor powders before/after heat treatment at 690 °C for 30 min.